LA-6104-MS
Informal Report

UC-78 and UC-34
Reporting Date: September 1975
Issued: November 1975

Numerical Calculation of Flashing from Long Pipes Using a Two-Field Model

by

William C. Rivard
Martin D. Torrey

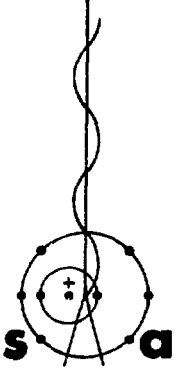

los alamos
scientific laboratory
of the University of California
LOS ALAMOS, NEW MEXICO 87545

UNITED STATES
ENERGY RESEARCH AND DEVELOPMENT ADMINISTRATION
CONTRACT W-7405-ENG. 36

In the interest of prompt distribution, this report was not edited by the Technical Information staff.

This work was supported by the Nuclear Regulatory Commission, Division of Reactor Safety Research.

Printed in the United States of America. Available from
National Technical Information Service
U S Department of Commerce
5285 Port Royal Road
Springfield, VA 22151
Price: Printed Copy $4.00 Microfiche $2.25

SYMBOLS

A	ratio of vapor/liquid volume fraction to bubble/droplet radius
a_ℓ	adiabatic sound speed for the liquid
C_d	drag coefficient
C_p	constant pressure specific heat for the vapor
C_{ps}	constant pressure specific heat for saturated vapor
C_ℓ	specific heat of the liquid
D	pipe diameter
$(E_v)_{cond}$	heat conduction term for the vapor internal energy equation
$(E_\ell)_{cond}$	heat conduction term for the liquid internal energy equation
F	resistive force per unit of mixture volume due to wall friction acting on the mixture
F_v	resistive force per unit of mixture volume due to wall friction acting on the vapor
F_ℓ	resistive force per unit of mixture volume due to wall friction acting on the liquid
f_v	pipe wall friction factor for the vapor
$(f_v)_{vis}$	viscous stress term for the vapor momentum equation
f_ℓ	pipe wall friction factor for the liquid
$(f_\ell)_{vis}$	viscous stress term for the liquid momentum equation
H_v	specific enthalpy of the vapor
H_{sv}	specific enthalpy of the saturated vapor
I_{sv}	specific internal energy of saturated vapor, a function of pressure
I_v	specific internal energy of the vapor
J_c	rate of production of liquid mass (or loss of vapor mass) per unit of mixture volume by condensation.
J_e	rate of production of vapor mass (or loss of liquid mass) per unit of mixture volume by evaporation.
K	interfacial friction function, related to the exchange of momentum between fields
k_s	related to the roughness of the pipe, k_s/D is the relative sand roughness (see Ref. 6 p.529).
L	latent heat of vaporization
N	number of bubbles/droplets per unit of mixture volume
p	pressure, assumed to be locally in equilibrium between the two fields
p_o	reference pressure for the liquid equation of state
Q	specific turbulent kinetic energy, $Q = 1/2\ (0.1\, v_\ell)^2$
q	specific turbulent kinetic energy, $q = 1/2\ [0.1\ (v_v - v_\ell)]^2$
R	heat exchange function, related to the exchange of internal energy between fields
r	bubble/droplet radius
R_e	Reynolds number
R_u	universal gas constant

s	characteristic eddy size
T_s	saturation temperature at the pressure p
T_v	vapor temperature
T_ℓ	liquid temperature
$\underline{u}_v$	vapor velocity, u_v = radial component, v_v = axial component
$\underline{u}_\ell$	liquid velocity, u_ℓ = radial component, v_ℓ = axial component
$(W_v)_{vis}$	viscous work term for the vapor internal energy equation
$(W_\ell)_{vis}$	viscous work term for the liquid internal energy equation
X	Lockhart-Martinelli parameter that relates ϕ_v to ϕ_ℓ
A	function of pressure used in the determination of C_p
a_ℓ	molecular diffusivity of the liquid
γ	constant parameter in the vapor equation of state, $\gamma = 1.30$
γ_{sv}	function of pressure, related to the saturated vapor $\gamma_{sv} = 1 + p/\rho_{sv}(p)\, I_{sv}(p)$.
θ	volume of vapor per unit of mixture volume
ϕ_v	two-phase friction multiplier for the vapor
ϕ_ℓ	two-phase friction multiplier for the liquid
κ	effective conductivity of the liquid, accounts for both molecular and turbulent diffusion of thermal energy
κ_ℓ	molecular conductivity of the liquid
λ_c	constant for the condensation rate J_c
λ_e	constant for the evaporation rate J_e
ν	kinematic viscosity of the two phase mixture
ν_v	kinematic viscosity of the vapor
ν_ℓ	kinematic viscosity of the liquid
ρ	mixture density, $\rho = \rho_v' + \rho_\ell'$
$\rho_{\ell o}$	microscopic density of the liquid at the pressure p_o
ρ_{sv}	microscopic density of saturated vapor, a function of pressure
ρ_v	microscopic vapor density, vapor mass per unit of vapor volume
ρ_v'	macroscopic vapor density, vapor mass per unit of mixture volume, i.e., $\rho_v' \equiv \theta\rho$
ρ_ℓ	microscopic liquid density, liquid mass per unit of liquid volume
ρ_ℓ'	macroscopic liquid density, liquid mass per unit of mixture volume, i.e., $\rho_\ell' \equiv \rho_\ell (1-\theta)$
t	function of H_v and p used in the determination of the vapor temperature.

NUMERICAL CALCULATION OF FLASHING FROM LONG PIPES USING A TWO-FIELD MODEL

by

William C. Rivard and Martin D. Torrey

ABSTRACT

A two-field model for two-phase flows, in which the vapor and liquid phases have different densities, velocities, and temperatures, has been used to calculate the flashing of water from long pipes. The IMF (Implicit Multifield) technique is used to numerically solve the transient equations that govern the dynamics of each phase. The flow physics is described with finite rate phase transitions, interfacial friction, heat transfer, pipe wall friction, and appropriate state equations. The results of the calculations are compared with measured histories of pressure, temperature, and void fraction. A parameter study indicates the relative sensitivity of the results to the various physical models that are used.

I. INTRODUCTION

An accurate description of the transient dynamics of multidimensional two-phase flow is necessary in order to perform an accurate safety analysis for light water nuclear reactors. Such an analysis requires the usage of large, highly complex computer codes. Several such codes have been developed throughout the country under the auspices of the Nuclear Regulatory Commission (NRC). To evaluate these codes, several Standard Problems are being assembled by the NRC. Each problem is to be computed with the various codes and the results compared with measured data.

This report describes comparisons of calculated results using the KACHINA[1,2] code with the data of Edwards et al.[3] for Standard Problem No. 1. The results of a parameter study show the relative importance of the various models used in the code to describe the macroscopic effects of microscopic processes. The KACHINA code describes two-phase flow using separate sets of field equations for each phase. The vapor and liquid phases have different densities, velocities, and temperatures but the same pressure. References 1 and 2 give a detailed discussion of the field equations and a description of the IMF (Implicit Multifield) technique that is used for their numerical solution. Emphasis here is on the various models that are used to describe the fluid physics of steam-water mixtures relevant to Standard Problem No. 1. Specifically, these are the following:

1. Equations of state for steam and water allowing for compressibility of the liquid.
2. Finite rate phase transitions.
3. Finite rate interfacial heat transfer and friction.
4. Pipe wall friction.

The six field equations and the above models are described in Sec. II.

Standard Problem No. 1 involves the flash boiling of water from a long pipe closed at one end and suddenly opened to the atmosphere at the other by the rupture of a diaphragm. Initially the pipe is filled with water at a temperature of 515°K (467°F) and a pressure of 69.9 bars (1000 psig). The pipe is 410 cm (13.44 ft.) long with a 7.32 cm (2.88 in.)

inside diameter.

Edwards et al. have made quantitative measurements of pressure histories at several axial locations along the pipe wall and measurements of void fraction and temperature at a location 318.2 cm (10.44 ft.) from the open end. Comparisons of the calculated results with these measurements are made in Sec. III. The agreement is generally good.

The calculations have been performed by treating the region inside the pipe as one dimensional. Both one- and two-dimensional descriptions have been used for the region outside the pipe. No special conditions have been applied at the pipe exit. The solution inside the pipe is found to be insensitive to the detail of the description outside the pipe. A parameter study indicates that the solution inside the pipe is sensitive to the pipe wall friction and insensitive to the phase change rate, the interfacial heat transfer (temperature differences between the phases), and the interfacial friction (velocity differences between the phases).

II. THE TWO-FIELD MODEL

Separate sets of field equations are used for the liquid and vapor to describe the two-phase fluid dynamics. The field equations for the liquid are coupled to the field equations for the vapor through mass, momentum, and energy exchange and the assumption of pressure equilibrium.

A. Field Equations

The time-dependent, two-dimensional equations are as follows:

$$\frac{\partial \rho_v'}{\partial t} + \underline{\nabla} \cdot (\rho_v' \underline{u}_v) = J_e - J_c \quad , \tag{2.1}$$

$$\frac{\partial \rho_v' \underline{u}_v}{\partial t} + \nabla \cdot (\rho_v' \underline{u}_v \underline{u}_v) = - \theta \underline{\nabla} p + K(\underline{u}_\ell - \underline{u}_v) + J_e \underline{u}_\ell - J_c \underline{u}_v + (f_v)_{vis} \quad , \tag{2.2}$$

$$\rho_v' \frac{\partial I_v}{\partial t} + \rho_v' \underline{u}_v \cdot \underline{\nabla} I_v = - p \underline{\nabla} \cdot \left[\theta \underline{u}_v + (1-\theta)\underline{u}_\ell\right] + K(\underline{u}_\ell - \underline{u}_v)^2 + (J_e - J_c)\, p\left(\frac{1}{\rho_v} - \frac{1}{\rho_\ell}\right) + R(T_\ell - T_v) + (W_v)_{vis} + (E_v)_{cond} \quad , \tag{2.3}$$

$$\rho_v' = \rho_v \theta \quad , \quad \rho_\ell' = \rho_\ell (1-\theta) \quad , \tag{2.4}$$

$$\frac{\partial \rho_\ell'}{\partial t} + \underline{\nabla} \cdot (\rho_\ell' \underline{u}_\ell) = J_c - J_e \quad , \tag{2.5}$$

$$\frac{\partial \rho_\ell' \underline{u}_\ell}{\partial t} + \nabla \cdot (\rho_\ell' \underline{u}_\ell \underline{u}_\ell) = - (1-\theta) \underline{\nabla} p + K(\underline{u}_v - \underline{u}_\ell) + J_c \underline{u}_v - J_e \underline{u}_\ell + (f_\ell)_{vis} \quad , \tag{2.6}$$

$$\rho_\ell' \frac{\partial I_\ell}{\partial t} + \rho_\ell' \underline{u}_\ell \cdot \underline{\nabla} I_\ell = - (J_e - J_c)\left[p\left(\frac{1}{\rho_v} - \frac{1}{\rho_\ell}\right) + I_v - I_\ell\right] + R(T_v - T_\ell) + (W_\ell)_{vis} + (E_\ell)_{cond} \quad , \tag{2.7}$$

The source terms containing J_e and J_c that appear in these equations model the mass, momentum, and energy transfers associated with phase change. The terms associated with evaporation involve J_e and those associated with condensation involve J_c. In the mass conservation equations, Eqs. (2.1) and (2.5), evaporation produces vapor mass at the expense of liquid mass while condensation does the reverse. The mass exchange produces a momentum transfer between the phases according to Eqs. (2.2) and (2.6). The liquid momentum decreases upon evaporation at the rate $J_e \underline{u}_\ell$ while the vapor momentum increases at

this rate. Condensation, on the other hand, decreases the vapor momentum and increases the liquid momentum at the rate $J_c \underline{u}_v$. The specific internal energy of the vapor in Eq. (2.3) increases during evaporation as newly created vapor expands and compresses surrounding vapor. The specific internal energy of the liquid in Eq. (2.7) decreases during evaporation proportionally to the enthalpy difference between the vapor and liquid, which is the latent heat of evaporation for boiling between saturated states. During condensation the reverse effects occur.

These simple models are known to neglect many elements of the highly complex microphysics of phase change. For example, the whole process of momentum mixing and its associated energy dissipation is neglected. Also, no distinction is made between the thermodynamic state of newly created vapor and the state of the surrounding vapor or the state of newly condensed liquid and that of the surrounding liquid. The relative importance of the various microscopic processes must be determined through numerous careful calculations and comparisons with experimental data. It is our intention to develop the simplest possible models that adequately describe the essential physics related to the applications of interest.

B. Equations of State

The pressure p is related to the specific internal energy of the vapor I_v and the microscopic vapor density ρ_v for void fractions above a specified minimum value θ_o. When $\theta \leq \theta_o$ the mixture is treated as a compressible liquid, which is discussed later. For $\theta > \theta_o$ the temperature of the vapor T_v is determined from ρ_v and I_v while the temperature T_ℓ and the microscopic density ρ_ℓ of the liquid are determined from I_ℓ neglecting the small effects of pressure on the liquid state. Specifically, for $\theta > \theta_o$ the vapor equation of state relation is

$$p = \rho_v \left[(\gamma_{sv} - 1) I_{sv} - (\gamma - 1)(I_{sv} - I_v) \right] , \qquad (2.8)$$

where $\gamma_{sv}(p)$ and $I_{sv}(p)$ are obtained from analytic fits to data for saturated steam. These fits are given in the Appendix. The vapor temperature is determined from the constant pressure specific heat relation

$$H_v - H_{sv} = \int_{T_s(p)}^{T_v} C_p(T_v, p)\, dT_v , \qquad (2.9)$$

where $H_{sv}(p) = \gamma_{sv} I_{sv}$, $T_s(p)$ is the saturation temperature at the pressure p given in the Appendix, and C_p is given by

$$C_p(T_v, p) = \frac{\gamma R_u}{2(\gamma - 1)} \left\{ 1 + R_u T_v \left[(R_u T_v)^2 - 4\alpha p \right]^{-\frac{1}{2}} \right\} . \qquad (2.10)$$

The quantity α depends upon the pressure alone, i.e.,

$$\alpha(p) = (R_u T_s)^2 \left\{ 1 - \left[2(\gamma - 1) C_{ps} / \gamma R_u - 1 \right]^{-2} \right\} / 4p , \qquad (2.11)$$

where C_{ps} is the constant pressure specific heat of the saturated vapor given in the Appendix. Solution of Eq. (2.9) gives the vapor temperature directly as a function of p and H_v as

$$T_v = \frac{\tau}{2} + 2\alpha p / \tau R_u , \qquad (2.12)$$

where

$$\tau(H_v, p) = \frac{2(\gamma - 1)}{\gamma R_u} (H_v - H_{sv}) + T_s + (T_s^2 - 4\alpha p / R_u^2)^{\frac{1}{2}} . \qquad (2.13)$$

The liquid temperature and microscopic density are determined from I_ℓ through analytic fits to the water data, which are given in the Appendix.

For non-equilibrium vapor, i.e., vapor for which $T_v < T_s$, Eqs. (2.8) and (2.12) do not apply. In this case the following relations are used to determine p and T_v

$$p = \rho_v (\gamma_{sv} - 1) I_v , \qquad (2.14)$$

$$T_v = T_s + (H_v - H_{sv}) / C_{ps} . \qquad (2.15)$$

These relations and Eqs. (2.8) and (2.12) are identical for saturated vapor.

When $\theta \leq \theta_o$, the mixture is treated as a compressible liquid with a high interfacial heat transfer rate and interfacial friction. The pressure is related to the microscopic liquid density* as

$$p = p_o + a_\ell^2 (\rho_\ell - \rho_{\ell o}) \tag{2.16}$$

where p_o and $\rho_{\ell o}$ are reference values and a_ℓ is the adiabatic sound speed for the liquid (see the Appendix). In accord with the high interfacial heat transfer rate the vapor temperature is set equal to the liquid temperature, which is determined from I_ℓ. The pressure and vapor temperature determine I_v and ρ_v from the vapor equation of state. This procedure ensures that p is continuous across θ_o. In accord with high interfacial friction, the vapor velocity is set equal to the liquid velocity when $\theta \leq \theta_o$.

C. Phase Change Rates

The mass exchange between the vapor and liquid is governed by the evaporation and condensation rates J_e and J_c, respectively. These rates are determined by the following expressions

$$J_e = \lambda_e A \rho_\ell' \theta (T_s R_u)^{\frac{1}{2}} (T_\ell - T_s)/T_s \ , \quad \text{for } T_\ell \geq T_s$$

$$= 0 \ , \quad \text{otherwise} \tag{2.17}$$

$$J_c = \lambda_c A \rho_v' (1-\theta)(T_s R_u)^{\frac{1}{2}} (T_s - T_v)/T_s \ , \quad \text{for } T_v \leq T_s$$

$$= 0 \ , \quad \text{otherwise} \tag{2.18}$$

where A is proportional to the area of contact between the two phases per unit of mixture volume. For N equal size spherical bubbles or droplets per unit of volume, A is given by

$$A = \begin{cases} \theta^{2/3}(4\pi N/3)^{1/3} \ , & \theta \leq 1/2 \\ (1-\theta)^{2/3}(4\pi N/3)^{1/3} \ , & \theta > 1/2 \ . \end{cases} \tag{2.19}$$

*For application to Standard Problem No. 1, T_ℓ is essentially constant for $\theta \leq \theta_o$ so that the pressure depends only upon the density.

Equations (2.17) and (2.18) assume that the rate of energy transfer by diffusion within the liquid and vapor is large relative to the rate of energy exchange from phase change. In accord with this assumption, the bulk liquid and vapor temperatures are used to determine J_e and J_c. A better model in which the vapor production rate is controlled by the diffusion of thermal energy from the bulk liquid to the bubble interface is described and demonstrated in Sec. III.

D. Interfacial Friction

The momentum and energy exchange that results from the dynamic interaction of the vapor and liquid phases is modeled through the interfacial friction function K given by

$$K = \frac{3}{8} \rho \left[C_d |\underline{u}_v - \underline{u}_\ell| + \frac{12\nu}{r} \right] A \ , \tag{2.20}$$

where

$$\rho = \rho_v' + \rho_\ell' \ , \tag{2.21}$$

$$\nu = \theta \nu_v + (1-\theta)\nu_\ell \ , \tag{2.22}$$

$$r = \begin{cases} (3\theta/4\pi N)^{1/3} \ , & \theta \leq 1/2 \\ [3(1-\theta)/4\pi N]^{1/3} \ , & \theta > 1/2 \ , \end{cases} \tag{2.23}$$

and A is as defined in Eq. (2.19). In the limiting cases of $\theta \to 0$ and $\theta \to 1$, Eq. (2.20) approximates the friction between phases as the drag on a single bubble/droplet times the number of bubble/droplets per unit of mixture volume.

E. Heat Transfer

The exchange of thermal energy between the vapor and liquid is modeled through the heat exchange function R. The functional dependence of R upon fluid and thermodynamic variables is not restricted. The influences of extreme values of R were investigated to determine its relative importance for Standard Problem No. 1. Constant values of R large enough to produce equal temperatures between the phases and small enough to create large temperature differences (65°K) were considered.

F. Pipe Wall Friction

For one-dimensional calculations of flashing from long pipes, it is necessary to model the effects of wall friction. The resistive forces per unit of mixture volume acting on the vapor and liquid are

$$F_v = -\theta(f_v \rho_v v_v^2 \theta^2 / 2D)\Phi_v^2 \quad , \tag{2.24}$$

and

$$F_\ell = -(1-\theta)[f_\ell \rho_\ell v_\ell^2 (1-\theta)^2 / 2D]\Phi_\ell^2 \quad , \tag{2.25}$$

respectively. These force terms enter the momentum equations, Eqs. (2.2) and (2.6), through the terms $(f_v)_{vis}$ and $(f_\ell)_{vis}$. The multipliers Φ_v^2 and Φ_ℓ^2 are related through the Lockhart-Martinelli parameter X as

$$\Phi_v^2 = X \Phi_\ell^2 \quad , \tag{2.26}$$

where

$$X = \left[\frac{f_\ell \rho_\ell v_\ell^2 (1-\theta)^2}{f_v \rho_v v_v^2 \theta^2}\right]^{1/2} \quad . \tag{2.27}$$

The friction factors f_v and f_ℓ depend upon the Reynolds number and the pipe roughness through the relation[4]

$$f_{v,\ell}^{-1/2} = 1.74 - 2\log_{10}\left(2k_s/D + 18.7\, f_{v,\ell}^{-1/2}/R_e\right) \tag{2.28}$$

where the Reynolds number is $R_e = \theta v_v D/\nu_v$ for the vapor and $R_e = (1-\theta)v_\ell D/\nu_\ell$ for the liquid. The model is completely defined when Φ_ℓ^2 is specified. For the calculations described in the next section, two expressions for Φ_ℓ^2 have been considered

$$\Phi_\ell^2 = (\rho/\rho_\ell)(1-\theta)^2 \quad \text{and} \quad \Phi_\ell^2 = (1-\theta)^{-2} \quad . \tag{2.29}$$

Adding Eqs. (2.24) and (2.25) we obtain the resistive force per unit of mixture volume acting on the two-phase mixture. This force is respectively

$$F = -\frac{f_\ell \rho v_\ell^2}{2D} \quad \text{and} \quad F = -\frac{f_\ell \rho_\ell v_\ell^2}{2D} \tag{2.30}$$

using the expressions for Φ_ℓ^2 in Eq. (2.29).

III. NUMERICAL RESULTS

The KACHINA code numerically solves the two-field model described in Sec. II. The numerical methodology used in KACHINA is described in detail in Refs. 1 and 2. For the calculations reported here the 409.6-cm-long pipe is divided axially into 40 computational zones 10.24 cm in length. The sensitivity of the computational results to the number of zones in the pipe has been investigated by others[5] with the conclusion that 40 zones provide good spatial resolution. The region outside the pipe in the neighborhood of the open end has been calculated in one and two dimensions to assess the effects of exit conditions on the computed pressure histories within the pipe. Additional parameter studies include investigations of phase change rates, interfacial heat transfer, pipe wall friction, and interfacial friction.

The standard calculation is made with a single column of cells (one-dimensional everywhere), 40 cells inside the pipe and 5 cells outside. Outside the pipe, phase change is not permitted. The calculation required about 9 minutes of computer time on the CDC-7600. The initial data are as follows:

1. Inside the pipe
   a. $T_\ell = T_v = 502°K$ (444°F)*
   b. $p = 69.9$ bars (1000. psig)
   c. $\theta = 0.0001$
   d. $\rho_v = 3.93 \times 10^{-2}$ g/cm^3, $\rho_\ell = 0.831$ g/cm^3
   e. $u_v = u_\ell = 0$
   f. $N = 10$ bubbles per cm^3
   g. $C_d = 0.5$
   h. $k_s/D = 1.0 \times 10^{-3}$, which is typical for structural steel pipes

*The measured initial temperature is 515°K according to Ref. 3. A new phase change model is described later that allows the calculations to begin at this temperature.

i. The exit is fully open to flow, although Ref. 3 indicates a peripheral constriction was present that reduced the exit area by about 13%.

2. Outside the pipe

a. $T_\ell = T_v = 294°K$ (70°F), held fixed

b. $p = 1.0$ bar (14.7 psia), held fixed

c. $\theta = 0.9999$

d. $\rho_v = 6.3 \times 10^{-4}$ g/cm^3, $\rho_\ell = 0.935$ g/cm^3

e. $\underline{u}_v = \underline{u}_\ell = 0$

f. $N = 10$ droplets per cm^3.

The initial values of θ and N are arbitrary. Specification of θ as smaller than 0.0001 or greater than 0.9999 has a negligible effect on the results. The value of N has been varied between 1 and 1000. The effect of this variation on K is small since ν is small and r depends only on the cube root of N. The effect on the phase change rates is about a factor of 5 increase to a factor of 2 decrease in their values, which effects the details of the early pressure histories but has negligible effect at late times. The value of θ_o is set at $\theta_o = 0.008$.

The calculated results are compared with measured pressure histories in Figs. 1a - 1k. Comparisons with measured temperature and void fraction at station 5 are made in Figs. 1ℓ - 1m.

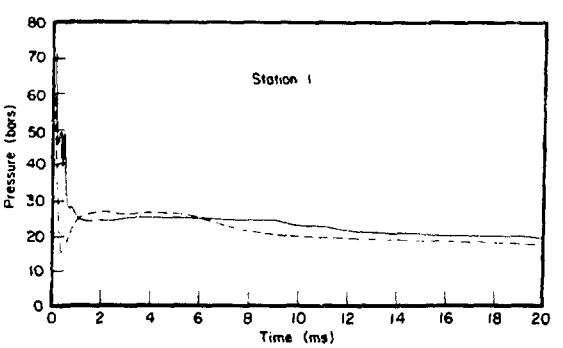

Fig. 1a. A comparison of KACHINA calculations (dashed line) with experimental data (solid line). Early time pressure history at Station 1, 16.8 cm from the open end.

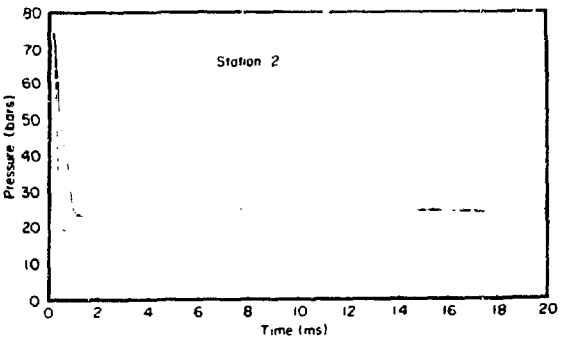

Fig. 1b. Early time pressure history at Station 2, 32.6 cm from the open end.

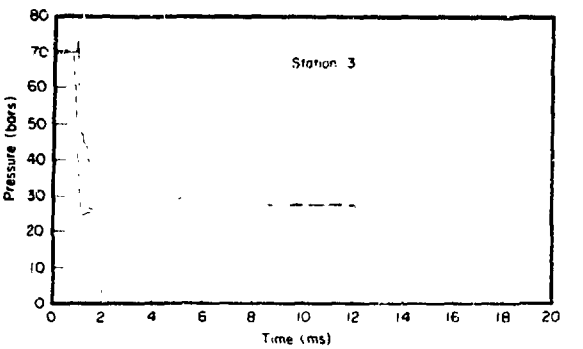

Fig. 1c. Early time pressure history at Station 3, 116.1 cm from the open end.

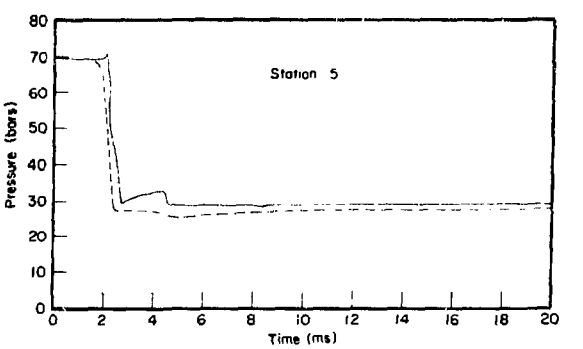

Fig. 1d. Early time pressure history at Station 5, 262.7 cm from the open end.

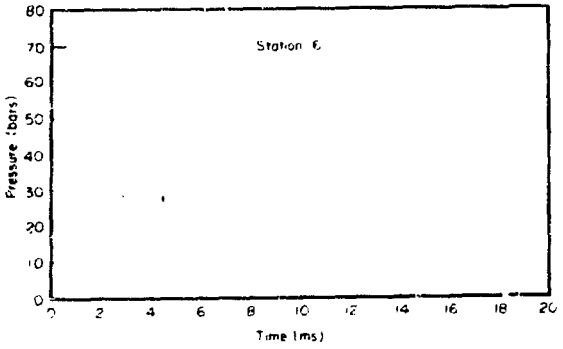

Fig. 1e. Early time pressure history at Station 6, 318.2 cm from the open end.

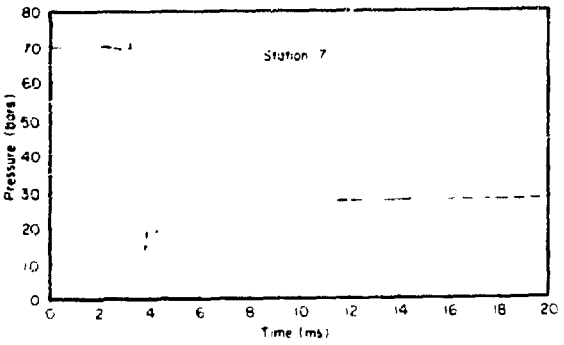

Fig. 1f. Early time pressure history at Station 7, 401. 7 cm from the open end.

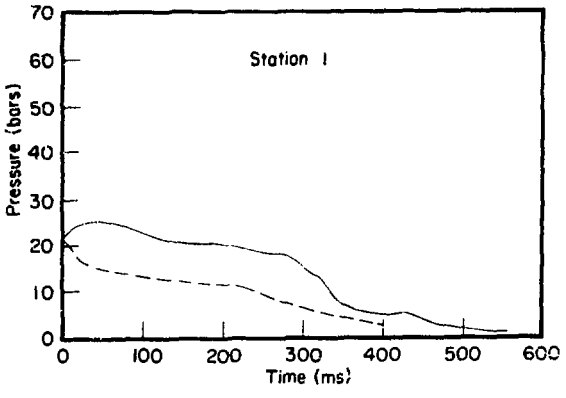

Fig. 1g. Late time pressure history at Station 1, 16.8 cm from the open end.

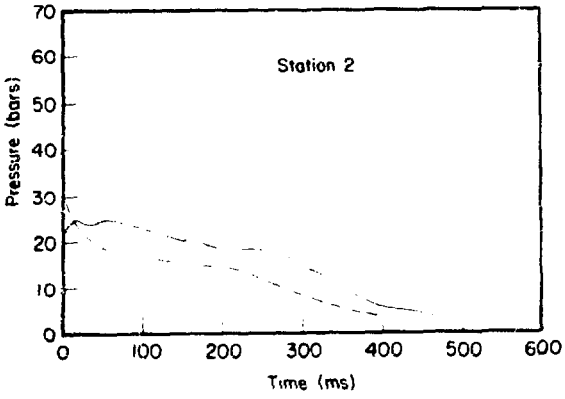

Fig. 1h. Late time pressure history at Station 2, 32.6 cm from the open end.

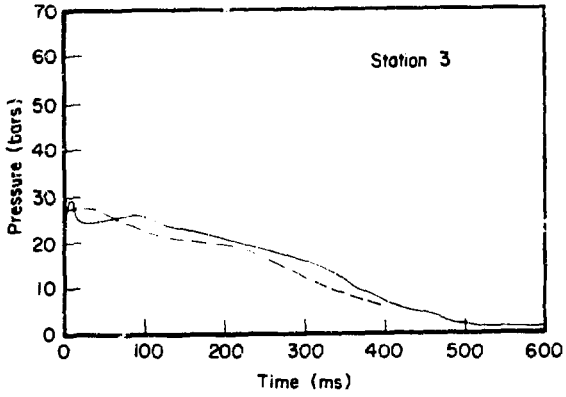

Fig. 1i. Late time pressure history at Station 3, 116.1 cm from the open end.

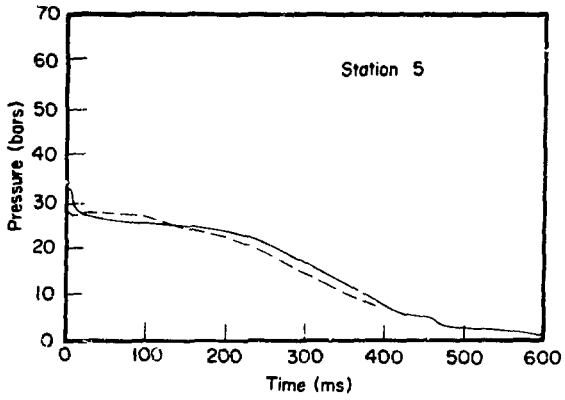

Fig. 1j. Late time pressure history at Station 5, 262.7 cm from the open end.

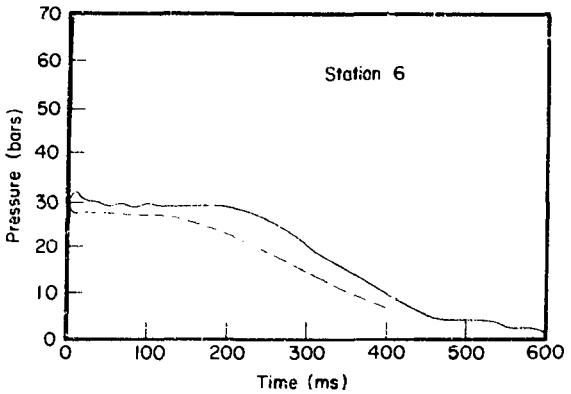

Fig. 1k. Late time pressure history at Station 6, 318.2 cm from the open end.

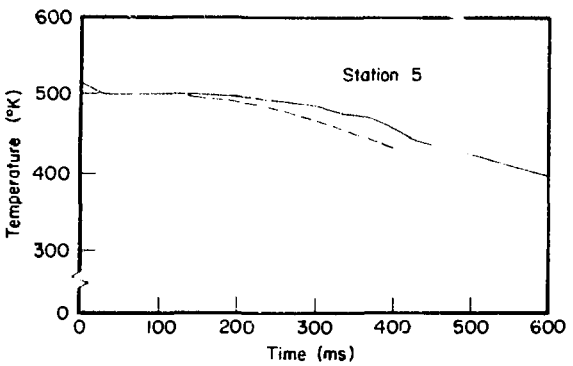

Fig. 1ℓ. Temperature history at Station 5, 262.7 cm from the open end.

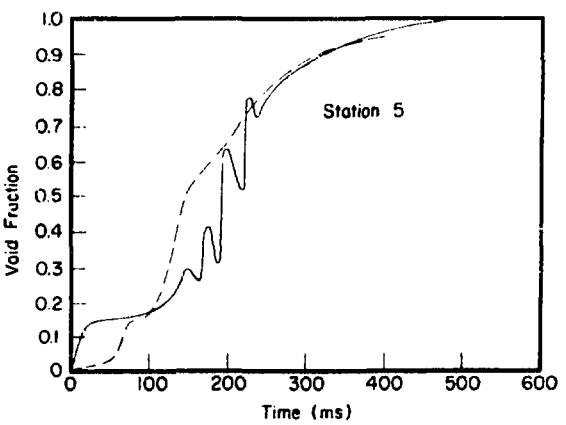

Fig. 1m. Void fraction history at Station 5, 262.7 cm from the open end.

To assess the effect of the exit region description on the pressure histories in the pipe, the full two-dimensional flow was calculated outside the pipe. The velocity fields for the vapor and liquid are shown in Fig. 2 for the exit region and a portion of the region inside the pipe. The pressure histories that were obtained differed by less than 0.7 bars (10 psi) from those obtained with the purely one-dimensional standard calculation. For the two-dimensional calculation, the pressure was held fixed at 1.0 bar along the right and top boundaries of the exit region and phase change was permitted outside the pipe.

The phase change rate multipliers, λ_e and λ_c, were chosen to approximate the early time pressure history at Station 7. Figure 3 shows the sensitivity of the calculated pressure histories at early time to variations in λ_e and λ_c over the range from 0.01 to 1. The value of 1.0 corresponds closely to an equilibrium phase change while the value of 0.01 gives a phase change rate that is clearly too slow

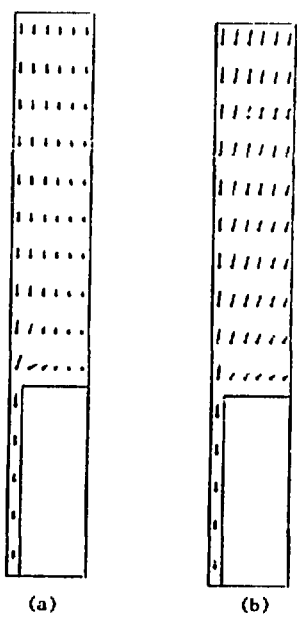

Fig. 2. Velocity vectors for the vapor (a) and liquid (b) in the exit region and a portion of the pipe. The length of the velocity vectors is proportional to the speed. The maximum vapor velocity is 23.9 cm/sec and the maximum liquid velocity is 16.4 cm/sec.

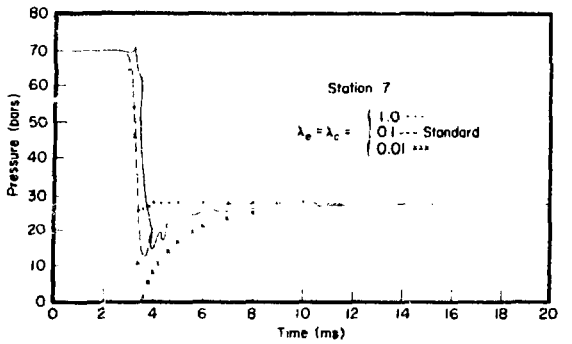

Fig. 3. Calculated early time pressure histories for various phase change rates compared to measured data (solid curve) at Station 7, 401.7 cm from the open end.

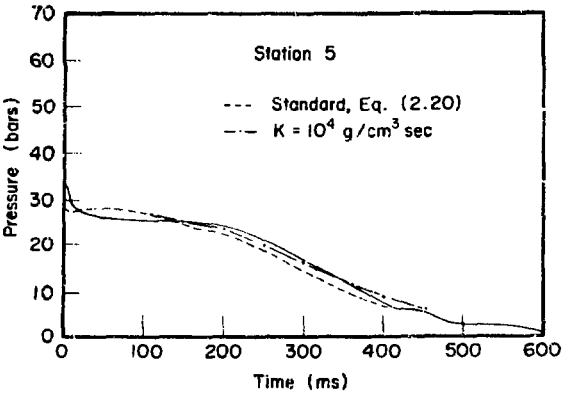

Fig. 4. Calculated late time pressure histories for two values of the interfacial friction coefficient compared to measured data (solid curve) at Station 5, 262.7 cm from the open end. The vapor velocity is typically 50% higher than the liquid velocity near the exit for the standard calculation and essentially the same as the liquid velocity for K = 10^4 g/cm^3-sec.

to match the early time data. The value of 0.1 was used to obtain the results shown in Figs. 1a - 1m. The calculated pressure histories at late times differ by less than 0.7 bars (10 psi) for λ_e and λ_c between 0.01 and 1.

The heat transfer rate between fields was varied to investigate the effects of unequal phase temperatures on the pressure histories. Differences in the vapor and liquid temperatures ranged from 2°K for large values of the heat transfer coefficient (R = 10^4) to 65°K for small values (R = 1). The effects on the calculated pressure histories was less than 0.7 bars. The results shown in Figs. 1a - 1m correspond to R = 10^4.

The effects on interfacial friction were investigated by considering a range of values for the momentum exchange function K. Calculations were performed for K as given by Eq. (2.20) and for a constant value of K = 10^4. In the first case, vapor velocities of 2.4 x 10^4 cm/sec and liquid velocities of 1.6 x 10^4 cm/sec were produced near the open end at a time of 100 ms. For the constant K = 10^4 the vapor and liquid velocities differed by less than 1.0 cm/sec for the entire blowdown. The calculated pressure histories are shown in Fig. 4 for Station 5. K was computed according to Eq. (2.20) to obtain the results presented in Figs. 1a - 1m.

The pipe wall friction models had the largest influence on the calculated pressure histories. The two models that were investigated are given in Eq. (2.29). The results are shown in Fig. 5 for Station 5 at late time. The pressure histories show negligible differences at early time. The results given in Figs. 1a - 1m were obtained with $\Phi_\ell^2 = (1-\theta)^{-2}$.

The results of the standard calculation differ most with the data near each end of the pipe. These differences are not sensitive to any of the parameter variations that have been considered and have also been noted for calculations performed with the SOLA-DF[6] code on this problem. A significant difference, which should not be overlooked at this point, is that the calculations have been performed for an initial liquid temperature of 502°K rather

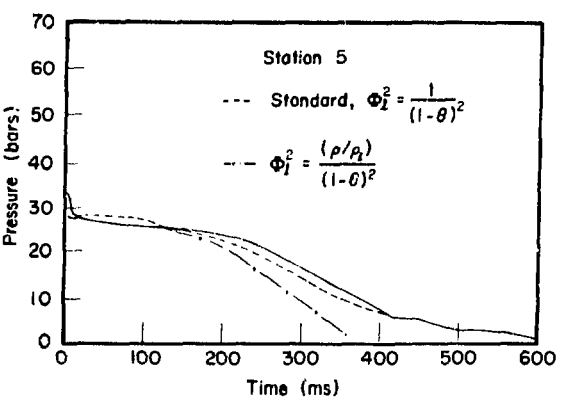

Fig. 5. Calculated late time pressure histories for two pipe wall friction models compared to measured data (solid curve) at Station 5, 262.7 cm from the open end.

than the measured value of 515°K. When the calculations are performed for this higher initial temperature the early time pressure histories approach 34.6 bars (502 psia), which corresponds to the saturation pressure at 515°K and is about 7 bars (100 psi) above the data. In Ref. 6 it is suggested that the liquid temperature at the bubble interface, rather than the bulk liquid temperature, controls the initial production of vapor. At later times when significant turbulence is generated it is postulated that the temperature difference between the interface and bulk liquid essentially vanishes and the bulk liquid temperature controls the boiling. Calculations performed in Ref. 6 with a model to represent this showed good agreement for the early time pressure histories and significantly improved the agreement at late time at Station 6. No improvement, however, was found near the open end of the pipe. This difference is discounted in Ref. 6 by the fact that calculations for another pipe diameter agree well with data near the open end. Based on this demonstration the model certainly appears to have merit but suffers from the fact that it required an a priori knowledge of the 13°K temperature difference.

A model is proposed here that will predict this temperature difference as a natural consequence. This model is based on the well-known relation for the asymptotic growth of a small bubble when the growth is controlled by conduction of heat from the bulk liquid to the bubble interface.[7] The asymptotic rate of bubble growth is given by

$$\frac{dr}{dt} = \frac{6\,\rho_\ell\, C_\ell\, \kappa}{\pi r}\left(\frac{T_\ell - T_G}{\rho_v L}\right)^2 . \qquad (3.1)$$

For simplicity at this stage of development, we neglect the initial inertia dominated growth associated with very small bubbles. The quantity κ is the effective thermal conductivity of the liquid. At early time it is the molecular conductivity. At late times it increases sharply as turbulence develops according to the relation

$$\kappa = \kappa_\ell + \kappa_\ell \left[0.05\, s\,(2Q)^{1/2}/\alpha_\ell + 0.005\, r_b\,(2q)^{1/2}/\alpha_\ell\right] . \qquad (3.2)$$

The two terms in the square bracket describe the effects of turbulence on the transfer of thermal energy. The term on the far right accounts specifically for the effect of relative velocity between the phases where the characteristic eddy size scales to the bubble radius and q is the specific turbulent kinetic energy given by $q = 1/2\,[0.1(v_v - v_\ell)]^2$. The other term accounts for the effects of turbulence in the absence of relative velocity where the scale s is given by $s = D/20$ and $Q = 1/2\,(0.1\, v_\ell)^2$. The constants 0.05 and 0.005 are empirically determined relaxation rates.

With this model the rate of production of vapor density is

$$\frac{\partial \rho_v'}{\partial t} = \frac{18.0\, C_\ell\, \theta\, \rho_\ell\, \kappa}{\pi\, \rho_v}\left(\frac{T_\ell - T_s}{r\, L}\right)^2 .$$

The results of calculations are shown in Figs. 6a - 6b for early time at Station 7 and for late time at Station 6, respectively. The agreement with the data lends support to the model, which now allows us to perform predictive calculations directly from the measured initial data. The rate given by Eq. (3.3) shows a sensitivity to the initial bubble radius. Future research should hopefully allow us to bound some initial bubble radius from considerations of nucleating sites and the initial, inertia dominated, growth rate.

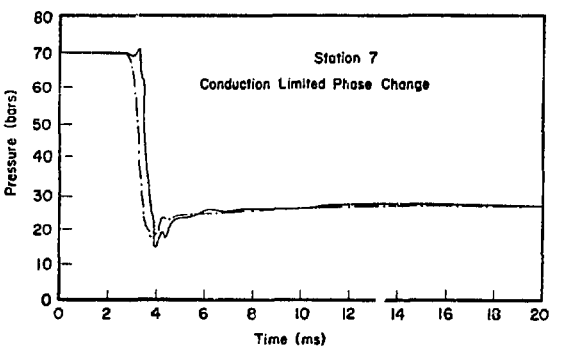

Fig. 6a. Calculated early time pressure history with the conduction limited phase change model compared with the measured data (solid curve) at Station 7, 201.7 cm from the open end.

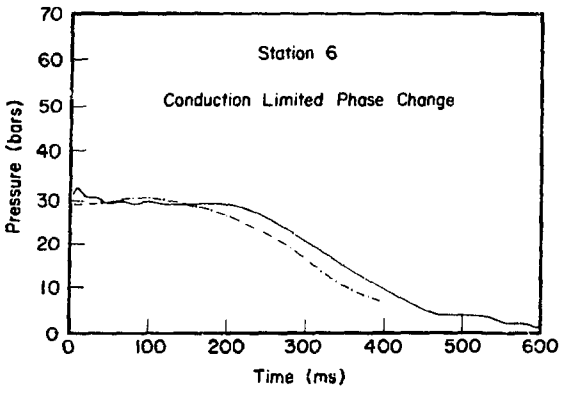

Fig. 6b. Calculated late time pressure history with the conduction limited phase change model compared to measured data (solid curve) at Station 6, 318.2 cm from the open end.

IV. SUMMARY

Two effects were investigated with the KACHINA code that could not be investigated with the drift model used in Ref. 5, namely, large relative velocities and large temperature differences between the phases. The calculated results, however, were not sensitive to either of these effects and hence the drift flux model and the two-field model gave essentially the same results. This should be expected for this problem, since the one-dimensional zones in the pipe necessarily result in mixture dynamics determined essentially by the liquid and only very slightly by the vapor. Furthermore, the pressure field is largely determined by the liquid temperature due to phase change so that the vapor temperature and density are nearly inversely related. For problems where the phases are separated or where they dynamically interact and have much different temperatures, we would expect the two-field description to be superior to the drift model. In application to reactor safety analysis these situations are likely to arise, for example, in the downcomer during emergency cooling.

APPENDIX

EQUATION OF STATE FUNCTIONS AND PARAMETERS

The various functions and parameters that are presently being used to describe the equations of state for steam and water are given here. These functions and parameters relate to Eqs. (2.8) - (2.16). The constants given are in (g - cm - sec - °K) units with pressure in dynes/cm^2. Comparisons of calculated state properties with steam table data are given in Tables A-I through A-III. Table A-I gives the comparisons for saturated steam, while Tables A-II and A-III give the results for superheated steam and subcooled water, respectively.

$$\gamma_{sv} = \begin{cases} 1.0666 + 1.02 \times 10^{-9} p - 2.548 \times 10^{-17} p^2, & p \leq 2.0 \times 10^7 \\ 1.0764 + 3.625 \times 10^{-11} p - 9.063 \times 10^{-19} p^2, & p > 2.0 \times 10^7 \end{cases}$$

$$I_{sv} = \begin{cases} 2.6194 \times 10^{10} - 4.995 \times 10^{15}/(3.403 \times 10^6 + p), & p \leq 2.0 \times 10^7 \\ 2.5896 \times 10^{10} + 6.35p - 1.0583 \times 10^{-7} p^2, & p > 2.0 \times 10^7 \end{cases}$$

$\gamma = 1.30$

$$T_s = 117.8\ (10^{-6}p)^{0.223} + 255.2$$

$$C_{ps} = 9.5875 \times 10^{6}\ (1.0 - T_s/647.3)^{-0.8566}$$

$$\nu_v = 0.2\ (10^{-6}p)^{-0.8426}$$

$$P_o = 6.992 \times 10^{7}$$

$$\rho_{\ell o} = 0.831$$

$$a_\ell = 1.234 \times 10^{5}$$

$$\nu_\ell = \begin{cases} 2.950 \times 10^{-3}\ (10^{-6}p)^{-0.2159}, & p \leq 1.5 \times 10^{7} \\ 2.178 \times 10^{-3}\ (10^{-6}p)^{-0.1038}, & p > 1.5 \times 10^{7} \end{cases}$$

$$\kappa_\ell = 6.2 \times 10^{4}$$

$$T_\ell = 273.0 + 99.65\ (2.402 \times 10^{-10} I_\ell) + 0.4830\ (2.402 \times 10^{-10} I_\ell)^2$$

$$- 0.4168\ (2.402 \times 10^{-10} I_\ell)^3 + 0.1183\ (2.402 \times 10^{-10} I_\ell)^4$$

$$\rho_\ell = [1.1171 - 0.2789\ (2.402 \times 10^{-10} I_\ell) + 0.2895\ (2.402 \times 10^{-10} I_\ell)^2$$

$$- 0.0994\ (2.402 \times 10^{-10} I_\ell)^3 + 0.0146\ (2.402 \times 10^{-10} I_\ell)^4]^{-1}$$

TABLE A-I

COMPARISON OF CALCULATED PROPERTIES WITH STEAM TABLE DATA FOR SATURATED STEAM

$P \times 10^{-6}$	T_s		$H_{sv} \times 10^{-10}$		$C_{ps} \times 10^{-7}$	
	Calc.	Data	Calc.	Data	Calc.	Data
1.01	373.3	373.0	2.676	2.676	2.002	2.034
4.76	422.0	423.0	2.740	2.745	2.368	2.320
15.55	472.4	473.0	2.798	2.791	2.942	2.883
39.78	523.0	523.0	2.797	2.800	3.942	3.918
85.93	573.2	573.0	2.753	2.751	6.139	6.148
165.35	623.2	623.0	2.544	2.568	16.065	15.8

TABLE A-II

COMPARISON OF CALCULATED PROPERTIES WITH STEAM TABLE DATA FOR SUPERHEATED STEAM

ρ_v	$I_v \times 10^{-10}$	$P \times 10^{-6}$		T_v	
		Calc.	Data	Calc.	Data
5.16×10^{-4}	2.583	0.99	1.0	423.8	423.0
3.48×10^{-4}	2.889	0.99	1.0	634.0	623.0
4.30×10^{-3}	2.710	9.89	10.0	520.3	523.0
3.03×10^{-3}	3.041	9.98	10.0	727.8	723.0
1.93×10^{-2}	2.811	50.55	50.0	630.6	623.0
1.36×10^{-2}	3.181	50.71	50.0	849.4	823.0
4.46×10^{-2}	2.702	101.30	100.0	634.9	623.0
2.81×10^{-2}	3.144	101.10	100.0	875.1	823.0

TABLE A-III

COMPARISON OF CALCULATED PROPERTIES WITH STEAM TABLE DATA FOR SUBCOOLED WATER

$I_\ell \times 10^{-10}$	T_ℓ		ρ_ℓ	
	Calc.	Data	Calc.	Data
0.4178	373.2	373.0	0.9587	0.9599
0.5445	403.6	403.0	0.9365	0.9366
0.6731	434.4	433.0	0.9070	0.9093
0.8042	465.9	463.0	0.8731	0.8780
0.9393	498.6	493.0	0.8345	0.8419
1.0808	533.0	523.0	0.7884	0.7992

REFERENCES

1. F. H. Harlow and A. A. Amsden, "Numerical Calculation of Multiphase Fluid Flow," J. Comp. Phys. 17, 19 (1975).
2. A. A. Amsden and F. H. Harlow, "KACHINA: An Eulerian Computer Program for Multifield Fluid Flows," Los Alamos Scientific Laboratory report LA-5680 (1974).
3. A. R. Edwards and T. P. O'Brien, "Studies of Phenomena Connected with the Depressurization of Water Reactors," Jour. BNES 9, 125 (1970).
4. H. Schlicting, Boundary Layer Theory, 4th Edition, (McGraw-Hill, New York, 1960).
5. T. A. Oliphant and C. W. Hirt, "Numerical Resolution Studies for Standard Problem One," contained in Los Alamos Scientific Laboratory report "Transport Theory, Reactor Theory, and Reactor Safety" LA-6029-PR, April 1 through June 30, 1975, ed. by K. D. Lathrop (August 1975).
6. C. W. Hirt and N. C. Romero, "Application of a Drift Flux Model to Flashing in Straight Pipes," Los Alamos Scientific Laboratory report LA-6005-MS (1975).
7. J. G. Collier, Convective Boiling and Condensation, (McGraw-Hill, New York, 1972), pp.116-118.

☆ U.S. GOVERNMENT PRINTING OFFICE 1975—677-343 53